Estimating the spatial autocorrelation function for ultrasound scatterers in isotropic media

Jiang-Feng Chen,[a] James A. Zagzebski,[b] Fang Dong, and Ernest L. Madsen
Department of Medical Physics, University of Wisconsin-Madison, Madison, Wisconsin 53706

(Received 15 January 1998; accepted for publication 19 February 1998)

The autocorrelation function pertaining to spatial distributions of ultrasonic scatterers in soft tissue is believed to contain useful information related to tissue morphology. A simple processing method applied to radio-frequency echo signals estimates this function for a sample having isotropic scattering conditions. It utilizes backscattered echo signals from the sample and echo signals from a reference object having defined scattering properties. The ratio of the echo signal power spectrum from the sample to the echo signal power spectrum from the reference object is obtained, and corrected for attenuation differences between the two media. This yields a ''form factor'' for the sample, whose inverse Fourier transform is the autocorrelation function. The method was tested using tissue-mimicking samples for which spatial autocorrelation functions could be modeled from the dimensions of embedded scatterers. The shapes of the measured autocorrelation functions were in reasonable agreement with those estimated, although measured functions overestimated the function at small lag distances. Scatterer diameters estimated from the zeros of the autocorrelation function agreed to within 6% of expected values when the measurement system bandwidth satisfied minimal criteria.
[S0094-2405(98)00305-8]

Key words: ultrasound, scattering, autocorrelation function, form factor, phantoms, scatterer size, tissue characterization

I. INTRODUCTION

When an ultrasonic pulse propagates through tissues, echo signals are generated by inhomogeneities in mass density and/or compressibility. Echoes from tissues have characteristics of random signals and are responsible for the ''speckle'' pattern observed on clinical B-mode images. To describe the underlying scattering processes, both discrete and continuous scattering models have been applied to tissues. Discrete models are characterized by an average scatterer number density and a scatterer size, while continuous models are characterized by a spatial autocorrelation function. This function describes the similarity of the mass density and compressibility at two positions in the medium.

The spatial autocorrelation function contains information related to tissue morphology. Actual autocorrelation functions for tissues are not known, but assumed forms are often utilized in data reduction algorithms to calculate backscatter properties of tissues and to estimate scatterer sizes.[1–3]

This paper is concerned with determinations of the spatial autocorrelation function in tissues or tissuelike media. For a statistically isotropic scattering medium, the autocorrelation function can be obtained from backscattered echo signals by applying data reduction algorithms that account for measurement system dependencies.[4] Alternatively, here we utilize a reference phantom containing randomly distributed scatterers, whose sizes are much smaller than the ultrasonic wavelength, to account for system factors. The ratio of the echo signal power spectrum from the sample to the power spectrum from the reference phantom is used to compute a form factor for scatterers in the sample. The inverse Fourier transform of the form factor yields the spatial autocorrelation function. The principles of this approach are outlined in this paper, and results of initial tests are reported.

II. THEORY

A. General expression for the echo signal power spectrum

The analysis applies to the ''raw'' radio-frequency echo signals and not to ultrasound B-mode image data. Under the Born approximation, an expression for the scattered echo signal voltage at time t, due to an ultrasonic pulse insonifying an inhomogeneous medium, is given by[5]

$$V(t)=\int_{-\infty}^{\infty} d\omega\ T(\omega)B(\omega)\omega^2 e^{-i\omega t} \times \int\int\int_{\Omega} d\mathbf{r}\ \gamma(\mathbf{r})A^2(\mathbf{r},\omega). \quad (1)$$

In this equation, the quantity $\gamma(\mathbf{r})\equiv[\kappa(\mathbf{r})-\kappa_o]/\kappa_o-[\rho(\mathbf{r})-\rho_o]/\rho(\mathbf{r})$ symbolizes local values of the compressibility, $\kappa(\mathbf{r})$, and density, $\rho(\mathbf{r})$, in the medium at position $\mathbf{r}$, where κ_o and ρ_o are the corresponding mean values. Here Ω is the total volume of the scattering medium; $T(\omega)$ is a complex transfer function relating the net instantaneous force on the transducer at frequency ω to the detected voltage; $B(\omega)$ is a complex superposition coefficient allowing represention of the incident ultrasonic pulse at point $\mathbf{r}$; and $A(\mathbf{r},\omega)$ corresponds to the value of the ultrasonic beam profile at point $\mathbf{r}$.

 0094-2405/98/25(5)/648/8/$10.00

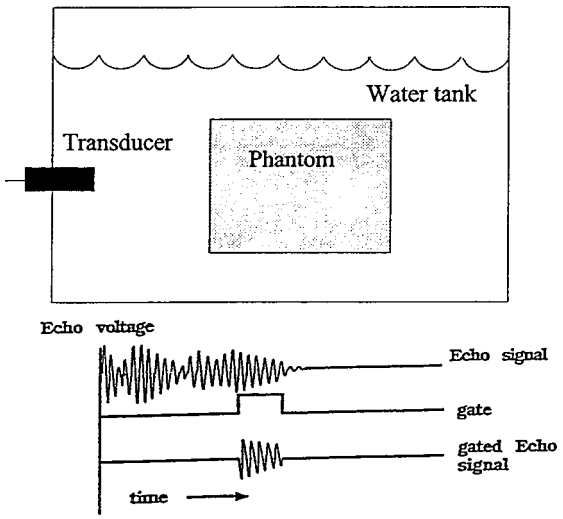

FIG. 1. Echo signal from a sample placed in water, with a time gate applied to isolate signals from a selected range.

Let us restrict our analysis to a segment of the echo signal defined by a time gate, as shown in Fig. 1. Its Fourier transform is given by

$$V_g(\omega)=\int_{-\infty}^{\infty} d\omega_1\ T(\omega_1)B(\omega_1)\omega^2 W(\omega-\omega_1) \times\int\int\int_{\Omega} d\mathbf{r}\ \gamma(\mathbf{r})A^2(\mathbf{r},\omega_1), \tag{2}$$

where $W(\omega-\omega_1)$ is the Fourier transform of the gating function.

If the gate duration is such that signals are selected from a region that is much longer than the characteristic length of the spatial autocorrelation function [i.e., the typical distance over which $\gamma(\mathbf{r})$ varies appreciably], Eq. (2) simplifies to

$$V_g(\omega)=T(\omega)B(\omega)\omega^2\int\int\int_{\Delta\Omega} d\mathbf{r}\ \gamma(\mathbf{r})A^2(\mathbf{r},\omega), \tag{3}$$

where $\Delta\Omega$ is the volume of the scattering medium which significantly contributes to the gated echo signal.

The echo signal power spectrum, obtained from the ensemble average of such signal segments, is given by

$$\begin{aligned} S(\omega,z)&=\langle V_g(\omega)V_g^*(\omega)\rangle \\ &=|T(\omega)B(\omega)|^2\omega^4\int\int\int_{\Delta\Omega} d\mathbf{r}_1\int\int\int_{\Delta\Omega} d\mathbf{r}_2 \\ &\quad\times A^2(\mathbf{r}_1,\omega)A^{*2}(\mathbf{r}_2,\omega)\langle\gamma(\mathbf{r}_1)\gamma^*(\mathbf{r}_2)\rangle \\ &=|T(\omega)B(\omega)|^2\omega^4\int\int\int_{\Delta\Omega} d\mathbf{r}_1\int\int\int_{\Delta\Omega} d\mathbf{r}_2 \\ &\quad\times A^2(\mathbf{r}_1,\omega)A^{*2}(\mathbf{r}_2,\omega)R(\mathbf{r}_1,\mathbf{r}_2), \end{aligned} \tag{4}$$

where $\langle\cdots\rangle$ denotes an ensemble average, $|...|$ represents the magnitude, z is the axial distance to the center of the gated region, and $R(\mathbf{r}_1,\mathbf{r}_2)\equiv\langle\gamma(\mathbf{r}_1)\gamma^*(\mathbf{r}_2)\rangle$ is the autocorrelation function of $\gamma(\mathbf{r})$. If the medium is isotropic and stationary, the autocorrelation function reduces to $R_\gamma(\Delta\mathbf{r})$ where $\Delta\mathbf{r}=\mathbf{r}_1-\mathbf{r}_2$ depends only on relative positions.

B. Local plane wave assumption

The representation for the transducer beam, $A(\mathbf{r},\omega)$, is computed by summing the contributions from each point on the transducer surface to the pressure at field point $\mathbf{r}$.[6] The expression takes into account attenuation in the medium, but the computation is simplified if the attenuation part can be separated from the integral. This simplification has been shown to yield accurate beam values when the distance from the transducer to the field point is greater than the diameter of the transducer.[7] In that case, we have

$$A(\mathbf{r},\omega)=e^{-\alpha(\omega)z}\int\int_S ds'\ \frac{e^{i\mathbf{k}\cdot(\mathbf{r}-\mathbf{r}')}}{|\mathbf{r}-\mathbf{r}'|}=e^{-\alpha(\omega)z}A_o(\mathbf{r},\omega), \tag{5}$$

where $\mathbf{k}$ points in the direction of wave propagation, $|\mathbf{k}|\equiv\omega/c$, c is the speed of sound, $\alpha(\omega)$ is the attenuation coefficient of the medium, and $\mathbf{r}'$ points to element ds' on the transducer surface. The origin of the coordinate system is taken to be at the center of the radiating element. In Eq. (5), $A_o(\mathbf{r},\omega)$ is $A(\mathbf{r},\omega)$ with $\alpha(\omega)=0$.

For the remainder of this paper we shall assume ''local plane wave'' conditions; i.e., the transducer beam pattern $A(\mathbf{r},\omega)$ does not vary significantly over the distance for which the spatial autocorrelation function decreases to negligible values. Thus we have

$$|A(\mathbf{r}_2,\omega)|\approx|A(\mathbf{r}_1,\omega)| \tag{6}$$

Assuming that the directions of $\mathbf{k}$, $\mathbf{r}_1$, and $\mathbf{r}_2$ are essentially the same and that $|\Delta\mathbf{r}|\ll|\mathbf{r}_1|\approx|\mathbf{r}_2|$, we can separate the tissue-dependent factors from instrumentation-dependent factors contributing to the power spectrum. We have

$$\begin{aligned} S(\omega,z)&\approx\left(|T(\omega)B(\omega)|^2\omega^4\int\int\int_{\Delta\Omega} d\mathbf{r}|A_0(\mathbf{r},\omega)|^4\right) \\ &\quad\times\left(e^{-4\alpha(\omega)z}\int\int\int_{\Delta\Omega} d\Delta\mathbf{r}\ e^{2i\mathbf{k}\cdot\Delta\mathbf{r}}R_\gamma(\Delta\mathbf{r})\right) \\ &=\left(|T(\omega)B(\omega)|^2\omega^4\int\int\int_{\Delta\Omega} d\mathbf{r}|A_0(\mathbf{r},\omega)|^4\right) \\ &\quad\times(e^{-4\alpha(\omega)z}S_\gamma(\mathbf{K})), \end{aligned} \tag{7}$$

where $\mathbf{K}=2\mathbf{k}$ and $S_\gamma(\mathbf{K})$ is the Fourier transform of the spatial autocorrelation function $R_\gamma(\Delta\mathbf{r})$. $S_\gamma(\mathbf{K})$ is called the ''form factor'' for scatterers in the medium. The form factor is the ratio of the scattering cross-section for a finite-sized scatterer to that for a point scatterer.[8] If the scatterers are pointlike (meaning they are much smaller than the ultrasonic wave length), the form factor is a constant.

C. Reference phantom method

The first factor on the right in Eq. (7) is an instrument-dependent factor, while the second factor, $(e^{-4\alpha(\omega)z}S_\gamma(\mathbf{K}))$,

depends on the properties of the sample. The former can be eliminated if we take ratios of the echo signal power spectrum from the sample at depth z to $S'(\omega,z)$, the echo signal power spectrum from the same depth in a reference medium whose speed of sound is approximately the same as that of the sample. This holds if the same instrumentation and control settings are used for both. Then we have for the sample form factor

$$S_\gamma(\mathbf{K}) \approx e^{4(\alpha(\omega)-\alpha'(\omega))z} \frac{S(\omega,z)}{S'(\omega,z)} S'_\gamma(\mathbf{K}), \tag{8}$$

where $S'_\gamma(\mathbf{K})$ and $\alpha'(\omega)$ are the form factor and the attenuation coefficient of the reference medium. After correcting for the difference between the attenuation coefficients of the two media and multiplying by the form factor of the reference phantom, the spatial autocorrelation function of the sample is determined using the inverse Fourier transform.

If the autocorrelation function of the sample is isotropic, the inverse Fourier transform can be simplified to

$$R_\gamma(\Delta r) = \int_0^{2\pi} d\phi \int_0^{\pi} d\theta \sin\theta \int_0^{\infty} dK\, K^2 S_\gamma(K) e^{iK\Delta r \cos\theta}$$

$$= 4\pi \int_0^{\infty} dK\, K^2 S_\gamma(K)\, \mathrm{sinc}\left(\frac{K\Delta r}{\pi}\right), \tag{9}$$

where $\mathrm{sinc}(x) = \sin(\pi x)/(\pi x)$ and $K = |\mathbf{K}| = 2|\mathbf{k}|$.

III. FREQUENCY BANDWIDTH REQUIREMENTS

Let us introduce the dimensionless parameters $y = Ka/2$ and $x = \Delta r/a$, where a is a ''characteristic length'' of the autocorrelation function; a may also be called an ''effective radius'' for scatterers in the medium.[1] Then Eq. (9) can be rewritten

$$R_\gamma(x) = \frac{32\pi}{a^3} \int_0^{\infty} dy\, y^2 s_\gamma(y) \mathrm{sinc}\left(\frac{2xy}{\pi}\right), \tag{10}$$

where $s_\gamma(y) \equiv S_\gamma(2y/a)$. Because the frequencies available in a typical measurement system are limited, it is important to consider the bandwidth required to determine a spatial autocorrelation function correctly. This limitation can be expressed using

$$R_\gamma(x) \simeq \frac{32\pi}{a^3} \int_{y_1}^{y_2} dy\, y^2 s_\gamma(y) \mathrm{sinc}\left(\frac{2xy}{\pi}\right), \tag{11}$$

where y_1 and y_2 depend on the lower and the upper frequency band-limits of the measurement system. Because the integrand becomes insignificant at both very low frequencies (due to the y^2 factor) and very high frequencies (due to the form factor itself), it is possible to specify requirements for y_1 and y_2 if limits can be established on the characteristic length of the autocorrelation function. The lower limit on the integral, y_1, must be small enough to keep the result essentially the same as the result integrated from zero. Similarly, y_2 should be large enough that the resultant spatial autocorrelation function approaches the result when the integral is extended to infinity.

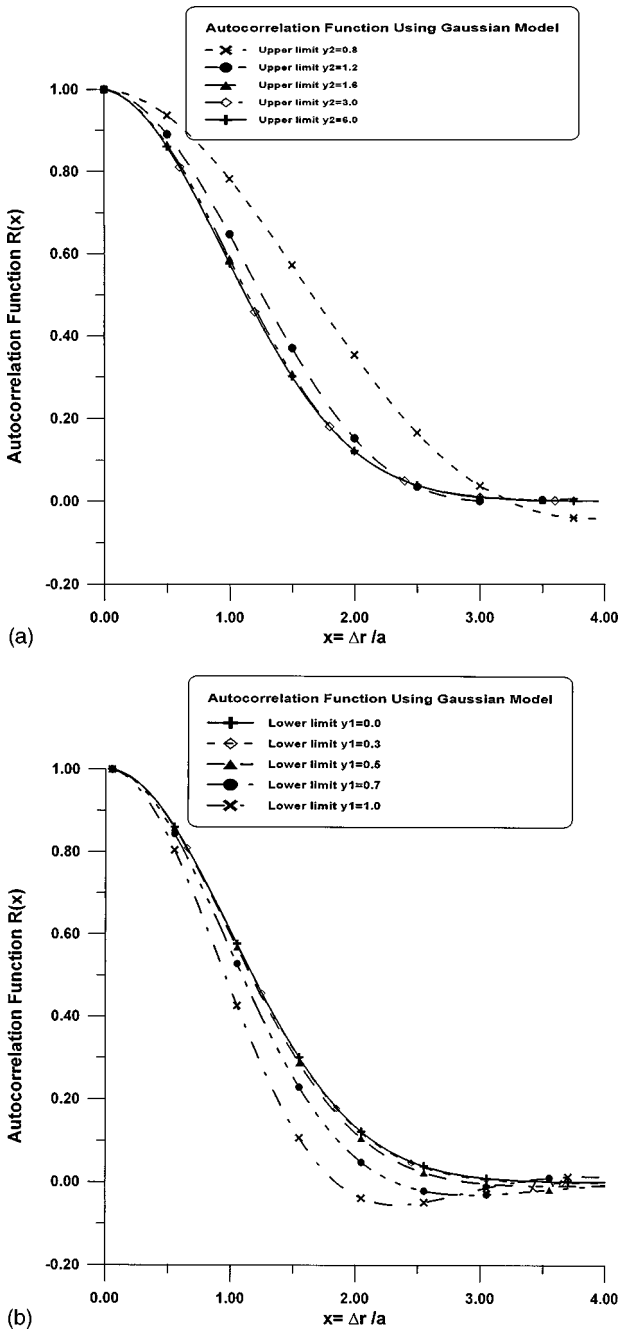

FIG. 2. Computed spatial autocorrelation function using the Gaussian form factor. Here a is a characteristic length of the correlation function. Part (a) illustrates the computed function for different values of y_2, which represents the upper frequency limit of the measurement system. Part (b) illustrates the function for different values of y_1, from the lower frequency limit.

Numerical calculations were used to assess requirements for y_1 and y_2 for simple autocorrelation models. Researchers have applied Gaussian, exponential, and fluid-sphere autocorrelation models when processing and analyzing backscatter data.[1–3] Form factors for these models[1,8] were substituted for $s_\gamma(y)$ in Eq. (11) and MATHCAD (1995 MathSoft Inc., Version 6.0) was used to evaluate the integral for different correlation distances and various values of y_1 and y_2.

Figures 2 and 3 present typical results. Figure 2(a) pre-

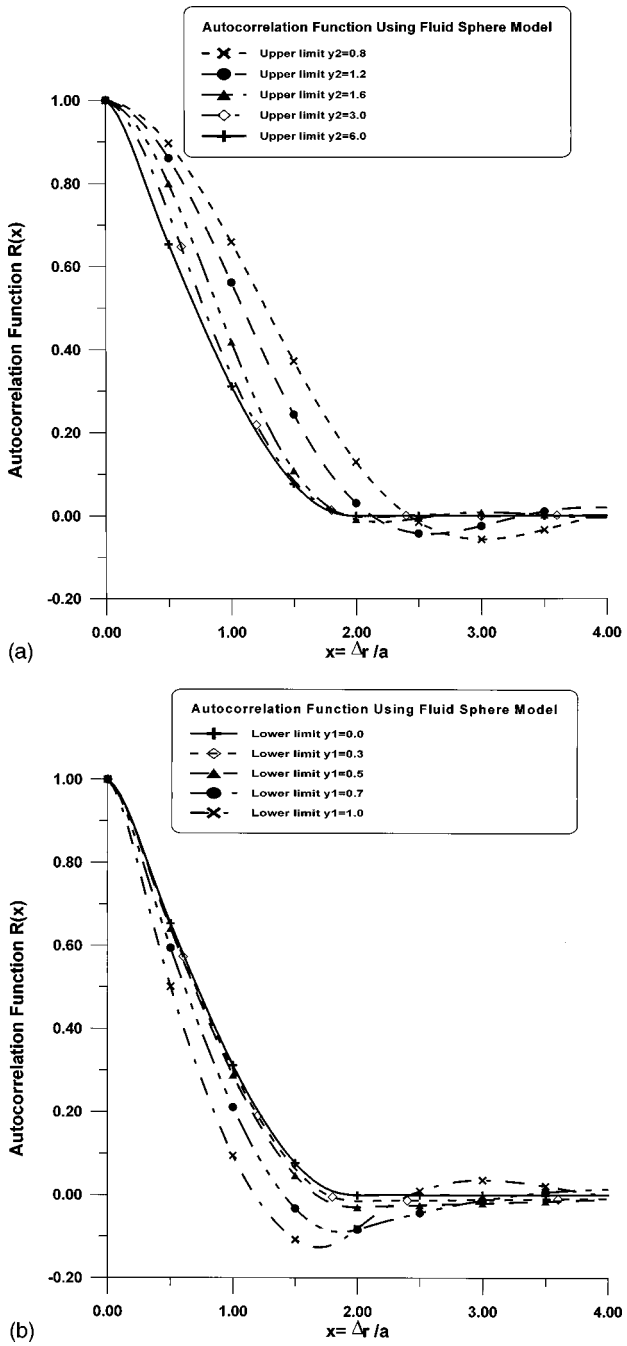

FIG. 3. Computed spatial autocorrelation function using the form factor for a ''fluid sphere.'' Here a is a characteristic length of the correlation function, in this case, the sphere radius. Part (a) illustrates the computed function for different values of y_2, which represents the upper frequency limit of the measurement system. Part (b) illustrates the function for different values of y_1, from the lower frequency limit.

sents computed autocorrelation functions for the Gaussian model when y_1 is held at 0 and y_2 varies from 0.8 to 6. With $y_2 \geqslant \approx 1.6$, the resultant spatial autocorrelation function is very close to the limit for $y_2 = 6$ or higher; i.e., the shape of the ''measured'' autocorrelation function is the same as the asymmptotic function, and its width at half max (WHM) is within 12% of that of the asymptotic function. Plots using different values of the lower frequency limit, y_1, are illustrated in Fig. 2(b). If y_1 does not extend to a sufficiently low frequency, the spatial autocorrelation function width will be underestimated; the measurement result may even exhibit ''ringing'' as shown for $y_1 = 0.7$ and higher. However, for $y_1 \leqslant 0.5$ the function is stable, i.e., curves are nearly identical to the curve for $y_1 = 0$.

Similar conclusions are drawn from simulations using the fluid sphere correlation model (Fig. 3). Here an appropriate measure of the scatterer size is $2a$, the scatterer diameter. The simulations indicate that one should strive for $y_1 \leqslant 0.5$ and $y_2 \geqslant 1.6$ if scatterer sizes, characterized by the first zero in the spatial autocorrelation function, are to be estimated. However, for the fluid sphere model, measuring details of the autocorrelation function for short lag distances requires higher frequencies, $y_2 \geqslant 3$ being more appropriate.

IV. INITIAL TESTS OF THE REFERENCE PHANTOM METHOD

A. Test samples

Three phantoms whose spatial autocorrelation functions could be predicted from the properties of the internal scatterers were used to evaluate the reference phantom method. The phantoms contain graphite or talc-loaded agar spheres randomly distributed in a background of plain agar. Spheres were produced using a ''shot-tower'' system described previously.[9] This technique yields gel spheres with a wide range of diameters, so the products of the shot tower were sieved to obtain spheres of the desired range. Figures 4(a)–4(c) present diameter distributions selected for scatterers in test phantoms labeled ''talc-1,'' ''talc-2,'' and ''ch1,'' respectively.

The spheres were introduced into 10.0 cm diameter, 4.0 cm thick cylinders containing molten agar. In each case, scatterers made up less than 10% of the volume of the sample, eliminating volume coherent effects from affecting the backscatter frequency dependence.[10] The contents of the cylinders were congealed with the samples rotating, assuring random distribution of spheres in the agar background.

A fourth sample, ''breast-GL,'' is a composite, representing ''glandular'' material used in ultrasound breast phantoms.[11] This material provided larger spheres, offering greater contrast in scatterer sizes than were achieved with samples 1–3. It consists of a distribution of clear agar spheres 0.6 to 1.2 mm in diameter, in a suspending matrix of an oil-in-gelatin emulsion.

The speed of sound and the attenuation coefficient in the test phantoms were measured using a narrow-band substitution technique.[12] Results are presented in Table I. The test phantoms are ''tissuelike'' in terms of the speed of sound. Sample ''ch1'' has a lower backscatter level and a lower attenuation coefficient than typical tissues. The remaining three (talc-1, talc-2, and breast-GL) have approximately tissuelike attenuation and backscatter levels.

The reference phantom used in these experiments contains glass bead scatterers with a mean diameter of 38 μm, randomly distributed in an agar background. The bead diameters are much smaller than the acoustic wavelengths (0.5 to

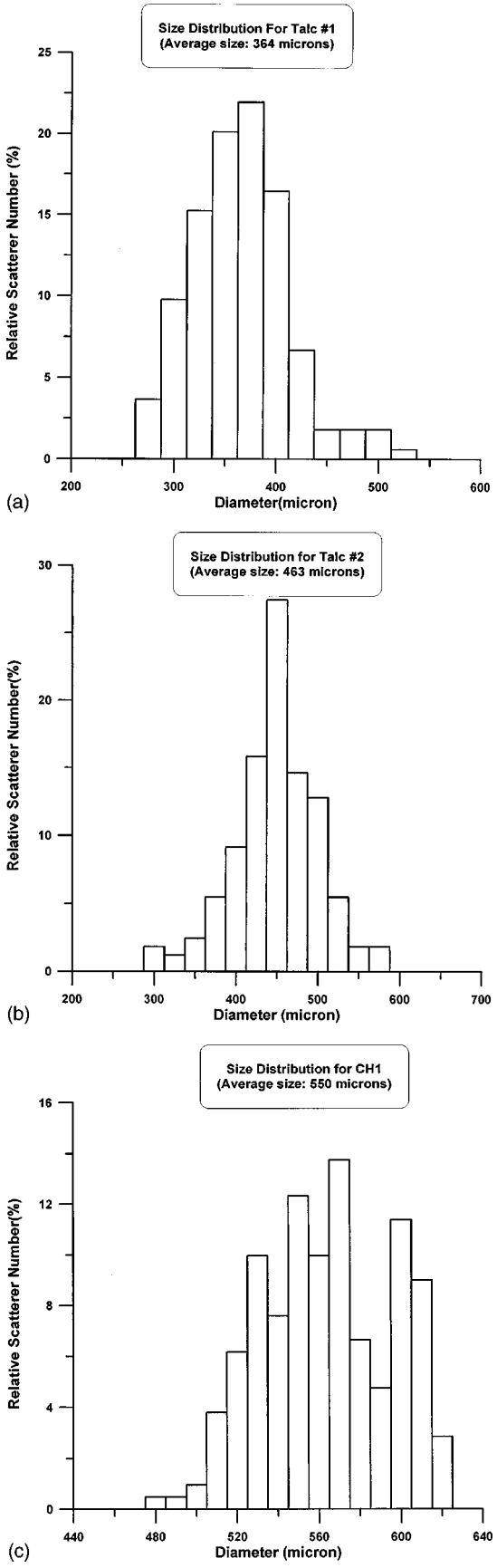

FIG. 4. Histograms showing scatterer size distributions for (a) talc-1, (b) talc-2, and (c) the ch1 phantom. Measurements were done using an optical microscope with a calibrated ocular micrometer to inspect excised pieces of test phantoms.

TABLE I. Properties of phantoms used to test the reference phantom method.

Phantom	Mean diam of scatterers (mm)	Speed of sound (m/s)	Attenuation (dB/cm) 1 MHz	Attenuation (dB/cm) 2 MHz
Reference	0.04	1580	0.163	0.516
talc-1	0.364	1544	0.22	0.44
talc-2	0.463	1545	0.22	0.44
ch1	0.55	1548	0.08	0.16
Breast GL	0.95[a]	1508	1.58	3.52

[a]Size distribution not available; 0.95 mm is an estimate.

3 mm for a 0.5 to 3 MHz frequency range), so the spatial autocorrelation function for the reference phantom is a delta function, and the form factor is a constant.

B. Echo data acquisition and signal processing

Echo data were acquired from test and reference phantoms while they were placed in degassed and distilled water. A 1.6 MHz broadband transducer was used to generate the ultrasonic pulses and receive echo signals. The transducer has a 19 mm diameter aperture and a 13.8 cm focal length. It was excited with single-cycle sine wave pulses, producing short duration acoustic pulses. Resultant echo signals were truncated using a 10.0 μs rectangular gate, digitized at 100 mega-samples per second with a digital oscilloscope (LeCroy 9400) and stored in a PC for off-line analysis. Signals were recorded for 100 statistically independent locations, realized by translating the sample perpendicularly to the transducer axis. The step size between transducer positions was 4.5 mm. Identical experimental conditions were used to record echo data for the reference phantom as were used for samples.

Discrete Fourier transforms were computed for each signal waveform. These were averaged to yield the echo signal power spectra for the sample and reference phantoms. Equation (8) was then used to correct for differences in attenuation between the sample and reference, yielding form factors for the samples. Spatial autocorrelation functions were obtained by taking the inverse Fourier transform of the form factors. The size (diameter) distributions of the scatterers in the talc-1, talc-2, and ch1 phantoms range from approximately 300 to 600 μm. The largest scatterers dictate the required lower frequency limit. Applying the condition $ka = 0.5$ with $a = 0.3$ mm yields a required low frequency, $f_{\text{low}} = (0.5 \times 1.54 \text{ mm}/\mu\text{s})/(2\pi \times 0.3 \text{ mm}) = 0.4$ MHz. Similarly, to reach the high frequency limit ($ka = 1.6$) for the smallest particle requires $f_{\text{hi}} = (1.6 \times 1.54 \text{ mm}/\mu\text{s})/(2\pi \times 0.150 \text{ mm}) = 2.6$ MHz. The frequency range available from the 1.6 MHz transducer was approximately 0.5 to 2.5 MHz.

Spatial autocorrelation functions for the samples were also modeled by assuming the scatterers could be described by an isotropic fluid sphere correlation function. For a sphere diameter of $2a$ this correlation function is given by[14]

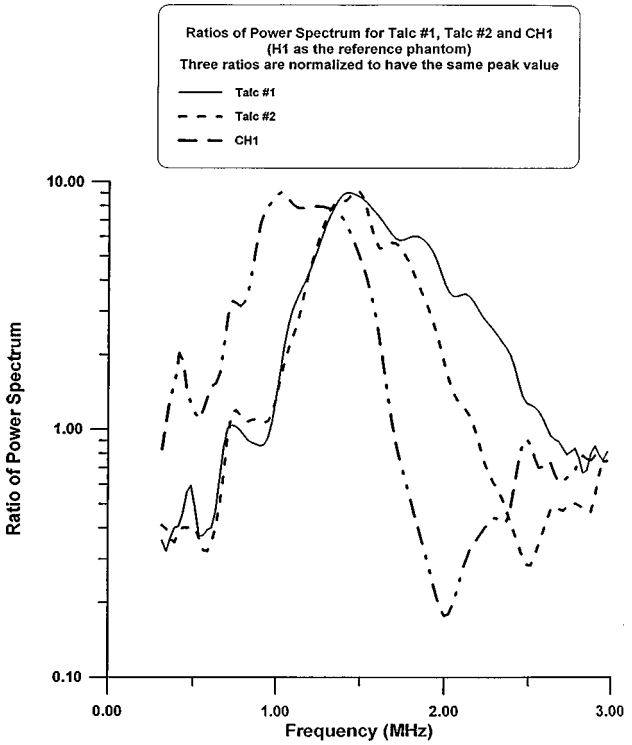

FIG. 5. Ratios of echo signal power spectra to the power spectrum from the reference phantom for the talc-1, talc-2, and ch1 phantoms.

$$R_{fs}(\Delta r)=\begin{cases} 1-\dfrac{3\Delta r}{4a}+\dfrac{(\Delta r)^3}{16a^3}, & 0\leqslant\Delta r\leqslant 2a, \\ 0, & \Delta r>2a. \end{cases} \tag{12}$$

To calculate a phantom's spatial autocorrelation function, Eq. (12) was applied for each sphere diameter. Then the scatterer diameter distribution was used to obtain a weighted contribution to the function for each scatterer size.

C. Results

Sample-to-reference phantom echo signal power spectrum ratios are shown in Fig. 5 for test phantoms, ch1, talc-1, and talc-2. It is interesting that the echo signal power spectra are easily distinguishable between the three phantoms, evidently related to the variations in scatterer size between the phantoms.

The measured spatial autocorrelation functions for the three samples are compared to fluid sphere model results in Figs. 6–8. The shapes of the measured autocorrelation functions are in reasonable agreement with model results. Obvious differences do exist, however, in that measured functions appear somewhat broader than the model predictions for the short lag distances, i.e., the full width at half maximum (FWHM) of the measured functions (Table II) are up to 24% greater than the calculated functions. We are not certain of the source of this discrepancy, but one possibility may be the upper frequency limit available with the 1.6 MHz transducer. Future studies will explore experimentally varying the frequency limits, hopefully complimenting the model studies.

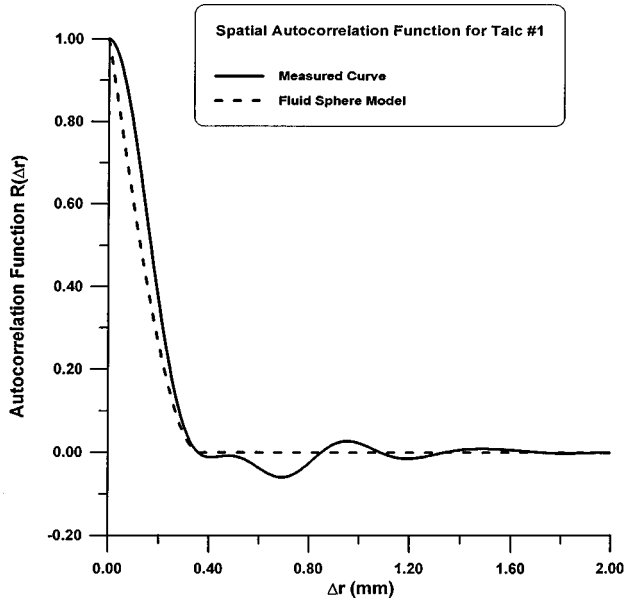

FIG. 6. Measured versus modeled spatial autocorrelation function for the talc-1 phantom.

For scatterers modeled as fluid spheres, a better measure of the scatterer ''size'' is the lag distance Δr for the SAF to decrease to zero. This should correspond to $\Delta r=2a$, the scatterer diameter. Comparing columns 4 and 5 in Table II, the measured and computed lag distances for the SAF to decrease to zero agree to within 6% for the ch-1, talc-1, and talc-2 samples.

Measured spatial autocorrelation function for all four test phantoms are presented in Fig. 9. The measured functions successfully arrange according to mean scatterer sizes in the test samples. Note, a diameter distribution was not available

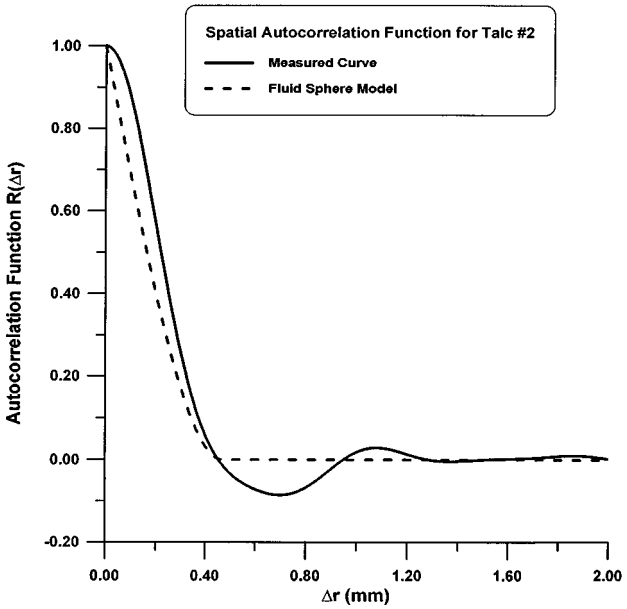

FIG. 7. Measured versus modeled spatial autocorrelation function for the talc-2 phantom.

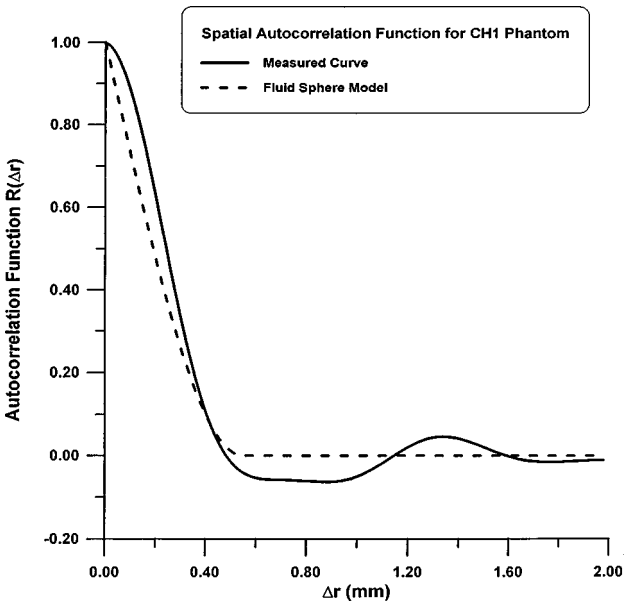

FIG. 8. Measured versus modeled spatial autocorrelation function for the ch1 phantom.

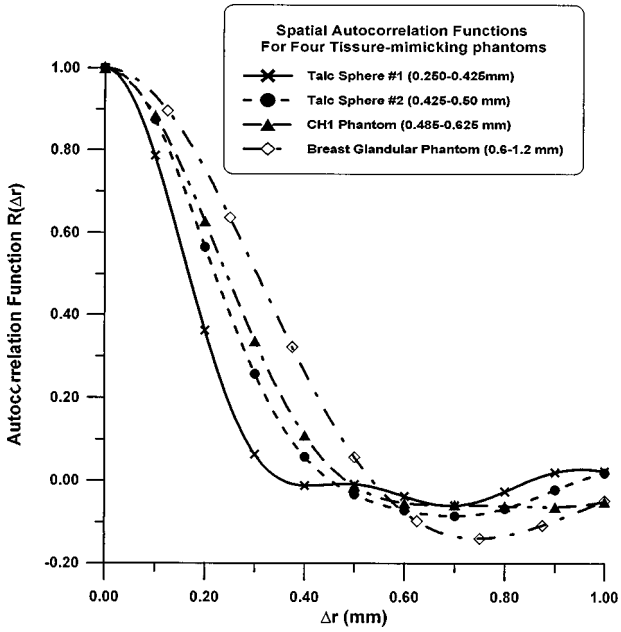

FIG. 9. Comparison of measured spatial autocorrelation functions for all four phantoms. The experimental frequency bandwidth was not sufficient for determining the SAF for the ''breast GL'' material, although its measured function is distinguishable from those of the other phantoms.

for the breast-GL material, but the size range includes spheres between 0.6 and 1.2 mm in diameter, selected by a sieving process. An estimate of the mean particle size for breast-GL is 0.95 mm. The lower frequency limit of the measurement was not sufficient to effectively determine a spatial autocorrelation function for this sample, but it is interesting to note that even with an insufficient bandwidth, the phantom is clearly distinguished from the others in this set.

V. DISCUSSION

The spatial autocorrelation function is fundamental to applications relating scattered ultrasound data to tissue microstructure.[1–4] Guidance to possible forms of this function for specific tissues can sometimes be gleaned from optical microscopy.[2,13] However, in most situations there is insufficient knowledge to specify the form of this function *a priori*. Parameters derived from ultrasound backscatter data, such as a ''correlation distance,'' will vary, depending on the assumed form of the autocorrelation function.[8]

This paper presents a method for estimating the spatial autocorrelation function for a sample in which it can be assumed that the function is isotropic. This is a reasonable assumption for many tissues, such as liver and spleen, although not for muscle, tendon, and kidney.[15,16] Any method for extracting acoustic properties of a medium from backscatter echo data must account for effects of the measurement system on these data. The reference phantom method described here is a relatively straightforward means to accomplish this. Thus, it may find applications using clinical instrumentation, where important instrumentation factors, such as the system transfer functions and the transducer beam characteristics, are not readily available.

TABLE II. Comparisons between measured and modeled/expected SAF results for the four test phantoms.

	FWHM (mm)		Width for SAF=0	
Phantom	Model	Measured	Expected	Measured
talc-1	0.13	0.17	0.364	0.355
talc-2	0.17	0.22	0.463	0.454
ch1	0.2	0.24	0.55	0.52
Breast GL	···	0.32[b]	0.95[a]	0.54[b]

[a]Size distribution not available; 0.95 mm is an estimate.
[b]Insufficient y_1 for the large scatterer sizes.

The results for a series of test phantoms suggest that this technique measures spatial autocorrelation functions with reasonable accuracy, providing the bandwidth of the measurement system is sufficient for the scatterers present. Here a broadband, 1.6 MHz center frequency transducer was used to acquire echo signals from a series of phantoms containing spherical scatterers. The reference phantom method was then applied to estimate the spatial autocorrelation function for each phantom. The lag distance for each measured spatial autocorrelation function to decrease to 0 agreed to within 6% of expected results based on the sizes and types (spheres) of scatterers in the phantoms. An exception to this was seen for the ''breast glandular'' material phantom, which contains larger scatterers than the other phantoms and for which the measured SAF underestimated the scatterer size. It is likely that the failure of the method to properly characterize the scatterer size in the breast glandular phantom is that the lower cutoff frequency of the transducer is insufficient.

Approximate agreement was found between shapes of measured and modeled autocorrelation functions for the phantoms. However, there was not as good a level of agreement for short lag distances, as judged by inspection of the

curves. In addition, the full widths at half-maximum amplitudes of measured SAFs were not in as close agreement with expected results as the first zero widths. Both of these shortcomings are believed to be caused by an insufficient high-frequency bandwidth of the experimental data. Future experimental testing will explore more fully the dependence of results on both lower and upper frequency limits of the measurement system. Methods for combining results of transducers of different frequencies also will be explored to investigate whether such an approach would improve these measurements.

VI. CONCLUSIONS

A method utilizing a reference phantom can provide effective determinations of the spatial autocorrelation function in tissuelike materials. Tests in phantoms yield measured autocorrelation functions whose total widths agree to within 6% of expected values. Frequency bandwidth limits can restrict the ability to determine the spatial autocorrelation function accurately.

ACKNOWLEDGMENTS

This work was support, in part, by the Wisconsin Clinical Cancer Center and by National Institute of Health Grant No. R01-CA39224. The assistance of G. Frank is gratefully acknowledged.

[a]Current address: Siemen's Medical Systems, Inc. P.O. Box 7002, Issaqua, WA 98029-7002.
[b]Address for correspondence: Department of Medical Physics, University of Wisconsin, 1300 University Avenue, Room 1530, Madison, WI 53706. Electronic mail: jimzag@macc.wisc.edu

[1]F. L. Lizzi, M. Ostromogilsky, E. J. Feleppa, M. C. Rorke, and M. M. Yaremko, ''Relationship of ultrasonic spectral parameters to features of tissue microstructure,'' IEEE Trans. Sonics Ultrason. **34**, 319–329 (1987).
[2]M. F. Insana, T. J. Hall, and J. L. Fishback, ''Identifying acoustic scattering sources in normal renal parenchyma from the anisotropy in acoustic properties,'' Ultrasound Med. Biol. **17**, 613–620 (1991).
[3]T. J. Hall, M. F. Insana, L. A. Harrison, and G. G. Cox, ''Ultrasonic measurement of glomerular diameters in normal adult humans,'' Ultrasound Med. Biol. **22**, 987–997 (1996).
[4]M. C. Macdonald, ''Determination of the spatial autocorrelation function of ultrasonic scatterers using the frequency dependence of backscattering,'' Ph.D. thesis, University of Wisconsin—Madison, 1992.
[5]J.-F. Chen, J. A. Zagzebski, and E. L. Madsen, ''Tests of backscatter coefficient measurement using broadband pulses,'' IEEE Trans. Ultrason. Ferroelectr. Freq. Control **40**, 603–607 (1993).
[6]E. L. Madsen, M. M. Goodsitt, and J. A. Zagzebski, ''Continuous waves generated by focused radiators,'' J. Acoust. Soc. Am. **70**, 1508–1517 (1981).
[7]L. X. Yao, J. A. Zagzebski, and E. L. Madsen, ''Backscatter coefficient measurements using a reference phantom to extract depth-dependent instrumentation factors,'' Ultrason. Imaging **12**, 58–70 (1990).
[8]M. F. Insana and D. G. Brown, ''Acoustic scattering theory applied to soft biological tissues,'' in *Ultrasonic Scattering in Biological Tissues*, edited by K. Shung and G. Thieme (CRC, Boca Raton, FL, 1991), p. 107.
[9]R. B. Chin, E. L. Madsen, J. A. Zagzebski, H. Jadvar, X. Wu, and G. R. Frank, ''A reusable perfusion supporting tissue-mimicking material for ultrasound hyperthermia phantoms,'' Med. Phys. **17**, 380–390 (1990).
[10]J.-F. Chen and J. A. Zagzebski, ''Frequency dependence of backscatter coefficient vs. scatterer volume fraction,'' IEEE Trans. Ultrason. Ferroelectr. Freq. Control **43**, 345–353 (1996).
[11]E. L. Madsen, F. Dong, J. A. Zagzebski *et al.*, ''Accurate simulation of in vitro breast tissue for anthropomorphic phantoms,'' J. Ultrasound Med. **15**(3), S66 (1996) (abstract).
[12]E. L. Madsen and J. A. Zagzebski, ''Oil-in-gelatin dispersions for use as ultrasonically tissue-mimicking materials,'' Ultrasound Med. Biol. **8**, 277–287 (1982).
[13]M. F. Insana and T. J. Hall, ''Parametric ultrasound imaging from backscatter coefficient measurements: image formation and interpretation,'' Ultrason. Imaging **12**, 245–267 (1990).
[14]F. E. Stanke, ''Spatial autocorrelation functions for calculations of effective propagation constants in polycrystalline materials,'' J. Acoust. Soc. Am. **80**, 1479–1485 (1986).
[15]J. G. Mottley and J. G. Miller, ''Anisotropy of the ultrasound backscatter of mayocardial tissue. I. Theory and measurement *in vitro*,'' J. Acoust. Soc. Am. **83**, 755–765 (1988).
[16]M. F. Insana, ''Modeling acoustic backscatter from kidney microstructure using an anisotropic correlation function,'' J. Acoust. Soc. Am. **97**, 649–655 (1995).